Liquid Crystals

ISSN: 0267-8292 (Print) 1366-5855 (Online) Journal homepage: https://www.tandfonline.com/loi/tlct20

Uniform and fast switching of window-size smectic A liquid crystal panels utilising the field gradient generated at the fringes of patterned electrodes

Kun Li, Mike Pivnenko, Daping Chu, Andrew Cockburn & William O'Neill

To cite this article: Kun Li, Mike Pivnenko, Daping Chu, Andrew Cockburn & William O'Neill (2016) Uniform and fast switching of window-size smectic A liquid crystal panels utilising the field gradient generated at the fringes of patterned electrodes, Liquid Crystals, 43:6, 735-749, DOI: 10.1080/02678292.2016.1142012

To link to this article: https://doi.org/10.1080/02678292.2016.1142012

Published online: 10 Feb 2016.

LIQUID CRYSTALS, 2016
VOL. 43, NO. 6, 735–749
http://dx.doi.org/10.1080/02678292.2016.1142012

Taylor & Francis
Taylor & Francis Group

Uniform and fast switching of window-size smectic A liquid crystal panels utilising the field gradient generated at the fringes of patterned electrodes

Kun Li[a], Mike Pivnenko[a], Daping Chu [a], Andrew Cockburn[b] and William O'Neill[b]

[a]Department of Engineering, Photonics & Sensors Group, Electrical Engineering Division, University of Cambridge, Cambridge, UK; [b]Department of Engineering, Centre for Industrial Photonics, Institute for Manufacturing, University of Cambridge, Cambridge, UK

ABSTRACT

A method to enable smectic A (SmA) liquid crystal (LC) devices to switch uniformly and hence fast from the clear state to a scattered state is presented. It will allow the reduction of the switching time for a SmA LC panel of 1×1 m^2 changing from a clear state to a fully scattered state by more than three orders to a few tens of milliseconds. Experimental results presented here reveal that SmA LC scattering initiates from the nucleated LC defects at the field gradient of the applied electric field usually along the edges of the panel electrode and grows laterally to spread over a panel, which takes a long time if the panel size is large. By patterning the electrodes in use, it is possible to create a large number of field gradient sites near the electrode discontinuities, resulting in a uniform and fast switching over the whole panel and the higher the pattern density the shorter the panel switching time. For the SmA LC panels used here, the ITO transparent electrodes are patterned by laser ablation and photolithography. It is shown that the defect nucleation time is much shorter than the growth time of the scattered region, hence it is possible to use the density of the field gradient sites to control the uniformity and switching time of a panel. Furthermore, the patterned SmA panels have a lower switching voltage than that of the non-patterned ones in general.

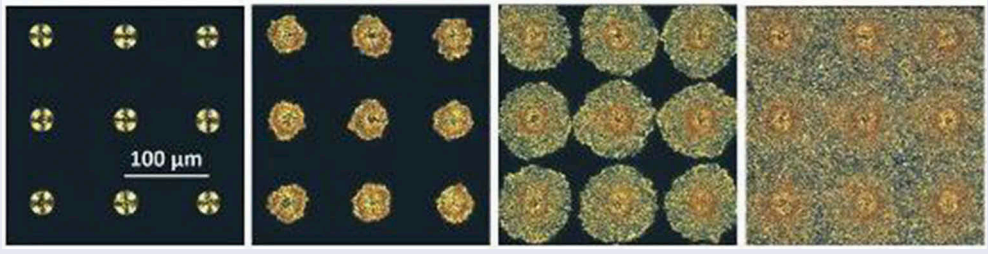

ARTICLE HISTORY
Received 23 November 2015
Accepted 11 January 2016

KEYWORDS
Smectic A liquid crystal; field gradient effect; scattering; patterned electrodes

1. Introduction

Large-size optically switching panels can enable a wide range of applications, from radiation control, ambient deco change to scattering media to information projection and display in the built environment both indoors and outdoors including privacy windows, building facades, and public information displays along motor ways and at transport hubs. These applications would require a large-size panel or panels made out of an energy-efficient material that can switch uniformly and fast.

Currently, some of such technologies, such as nematic polymer dispersed liquid crystal (PDLC) windows, have been used in aviation, automotive and cruise-ship sectors to provide a luxurious experience. For example, in year 2011, the cruise-ship Swift 141 was launched, it is the world's largest single project that is covered entirely with 3G (third-generation) PDLC switchable glasses; the windows reside in a scattered state and can be switched to clear by applying an electric voltage.[1]

Large-area ($<1 \times 2.8$ m^2) PDLC windows are already commercially available [2] and they are often used in buildings for artistic or privacy purposes. The continuous improvements are made on a number of practical aspects including the transmittance of the PDLC film and laminated glass at the UV and near-IR wavelength range, the UV durability by having an interlayer film for protection [3] and a self-adjusting smart window by doping a reverse-mode operation PDLC with photoconductive molecules.[4] Nevertheless a PDLC panel requires a constant electric field to maintain its clear

CONTACT Daping Chu dpc31@cam.ac.uk

state, resulting in a power consumption of ranging between 3.5 and 15.5 W/m^2.[2] Moreover, due to the nature of PDLC materials, there is a noticeable haze in the clear state of all the panels.[5]

Another competing technology for liquid crystal (LC)-based smart window which should be mentioned is related to the so-called polymer stabilised cholesteric textures (PSCTs).[6,7] It has a bi-stable mode which can maintain either clear or low-transmittance state without a voltage supply. However, the bi-stable mode of PSCT requires relatively high polymer concentration to stabilise a cholesteric texture, typically 8% as stated in Reference [8]. As a result, the outdoor durability of the device under direct sunlight is thought to be weak because of the polymer vulnerability under UV radiations. In addition, the switching speed for PSCT smart window is considered to be slow, in the range of several hundred milliseconds.[9,10] Long voltage pulses, in the order of 500 ms, are needed to switch the PSCT cell into the maximum and minimum transmittance states.[8] Together with other drawbacks such as high costs, difficulty in scaling-up and strong haze at a modest switching field, it is very challenging for PSCT to be widely adopted.[11]

Smectic A liquid crystal (SmA LC) panels provide an alternative with much improved performance because of the zero power maintenance of their optical states and no visible haze in the clear state.[12] There are no polarisers or alignment layers needed,[13] the same as in the case of PDLC. The stability of the optical states in zero electric field comes from a combined effect of the layered structure of the SmA phase, large defect activation energy and relatively high viscosity of the materials, enabling electro-optic devices such as energy efficient display panels and smart windows to be envisaged.[14] An early sample, a black-dyed SmA display test device, built in 1985 at Standard Telecommunications Laboratories still has its displayed contents retained after 30 years.[13]

Extensive works have been done by researchers and companies (Merck Group and Dow Corning Corp.) to enhance the stability of SmA LC mixtures over a wide temperature range for two types of SmA LCs: organic and siloxane-based LCs,[15–18] so that SmA LC windows can be operational in places of extreme weather conditions. SmA LC devices have also been demonstrated to have different levels of transmittance, from a few percent to above 80%, in the visible range.[13] The most of the absorption through the device in the clear state is actually from the indium-tin-oxide (ITO) layer and the plastic substrates if used. The absorption of the SmA LC material itself is minimal. In terms of UV stability, the siloxane-based SmA LC was expected to be at least similar or even superior to that of PDLCs,[14] and the colour pigment–doped SmA LC composites have been shown to have a life of more than 7 years under the full sun.[19]

The difference in the switching mechanisms between the PDLC and SmA LC materials means that the former can be switched within the order of 1–10 ms, while the latter can be cleared in a few milliseconds but scattered in a much longer period of time. The observational evidence suggests that the scattering of the SmA LC molecules usually starts from the edges of the device or the conductive electrode and propagates to the centre. Hence for a large panel of several metres across, the scattering time could be in the order of 1–10 seconds in total and the scattering itself will not be uniform across the panel. Although the speed of the scattering can be further increased by increasing the applied voltage, the effect is limited and it has the disadvantage of causing localised hot spots where arcing of the LC device occurs.

Attempts have been made to improve the SmA LC scattering time through material engineering, by doping the material with dielectric additives to increase possible defect nucleation sites.[13,20] However, the doping level has to be kept very low to maintain the integrity of the SmA LC materials and prevent it to become conductive.

This paper investigates the effect of the applied electric field on the scattering process and proposed a device structure with patterned electrodes for nearly size-independent fast and uniform scattering of SmA LC devices. The scattering process is observed with a polarising microscope to reveal the scattering initiation and propagation. The scattering time and transmittance in the scattered state are measured for different scattering voltages and different pattern densities. A defect generation mechanism is proposed for the scattering initiation in SmA LC devices. The scattering performances of organic and siloxane-based SmA LC devices are compared.

2. Experimental approach

2.1. LC materials, device preparation and electrode patterning

The LC devices used in this work consist of both the organic-based and siloxane-based SmA LC materials. The organic-based SmA LC is developed in-house using a cyanbiophenyl SmA LC composition, specifically a 4-cyano-4'-n-octyl biphenyl (8CB). The siloxane-based SmA LC is a proprietary LC provided by

Dow Corning Corporation (Midland, MI, USA).[21] The working temperature range is usually about 60°C, adjustable within −15 to ~66°C for the organic SmA LC and −40 to ~70°C [21] for the siloxane-based SmA LCs, by varying the material compositions.

A thin SmA LC layer (thickness d_c = 10 μm) was sandwiched between two ITO-coated glass substrates. The glass substrates are 1.1 mm thick and the ITO layer is about 21 nm thick and is in contact with the LC. The sheet resistance of ITO layer is ~100 Ω/□. The transmission of a single ITO-coated glass substrate is just above 90% in the visible range. The substrates were cleaned and assembled into working devices in a clean-room environment. The LC devices have an active region of 10 × 10 mm^2.

Two techniques were used to pattern the ITO electrode on a glass substrate, namely a laser ablation process and a photolithography process followed by a chemical etching. The laser process uses a single mode nanosecond pulsed fibre laser (G3 SM-S00044_1, SPI Lasers, Southampton, UK) of 1062 nm wavelength to remove the ITO layer directly without damaging the glass substrate underneath due to its negligible absorption. The fibre laser in use is driven by a scanning system (XLR8 x-y scan head from Nutfield Technology, Inc., Hudson, NY, USA), which generates patterned features and controls laser parameters through a software package (WaveRunner, Nutfield Technology, Inc.).

The photolithography process mainly consists of the use of an automated mask alignment system (EVG620, EV Group, St. Florian am Inn, Austria), a photo-resist (AZ5214E), a developer (AZ351B) and a photo mask. The size and the shape of the patterned features depend on the photo mask in use. A chemical etching step is needed after curing the photo resist to remove the selected ITO regions.

2.2. Patterned features

For the laser process, the diameter of the through holes on an electrode was set to be 30–35 μm in this study, as shown in Figure 1(a). The spatial profile of the laser output is Gaussian or Gaussian-like, and its central zone defines the minimum feature size for the actually removed materials, whereas the remainder of the incident beam merely contributes to the heat affected zone. In Figure 1(a), the through holes are substantially circular and positioned in a regular array. The hole density is described as the hole spacing value between any two adjacent ones in the x- and y-directions of the ITO electrode layer. Holes were patterned on one of the ITO-coated glass within the active area of 10 × 10 mm^2.

The laser process is also able to selectively remove a top section of the ITO layer to create a blind hole instead of a through hole, as shown in Figure 2(a) and 2(b), respectively, by controlling the laser energy output. The blind holes are of ~2 nm in depth and ~10 μm in diameter. The existence of blind holes is used to investigate if a surface roughness is able to initiate the uniform SmA LC scattering under similar driving conditions as the devices with through holes. Other patterns were produced on the ITO layer using the photolithography process with an example shown in Figure 2(c).

These patterns were measured with an Optical Profiler (Wyko NT1100, Veeco, Plainview, NY, USA) in the phase shifting interferometry mode. The depth of photolithography patterned features matches the ITO layer thickness of ~21 nm, while the depth of laser patterned through holes is around 12–13 nm as seen in Figure 2(d). The variation was due to the difference in the material removal mechanism. The photolithography process involves dissolving the exposed ITO in a chemical solution, while the contact

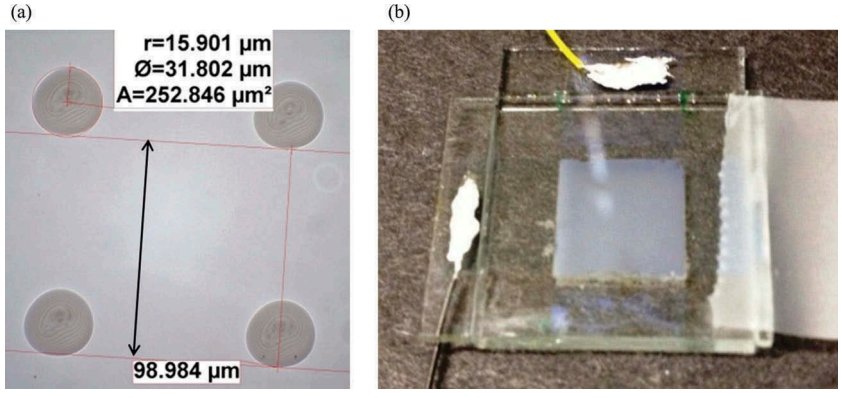

Figure 1. (colour online) (a) Laser patterned holes on an ITO-coated glass showing the hole dimension and the spacing. (b) SmA LC device (10 × 10 mm^2 active region) in a scattered state with patterns on one ITO-coated glass, consisting of a total of 10,000 holes of the same size and spacing as that in Figure 1(a).

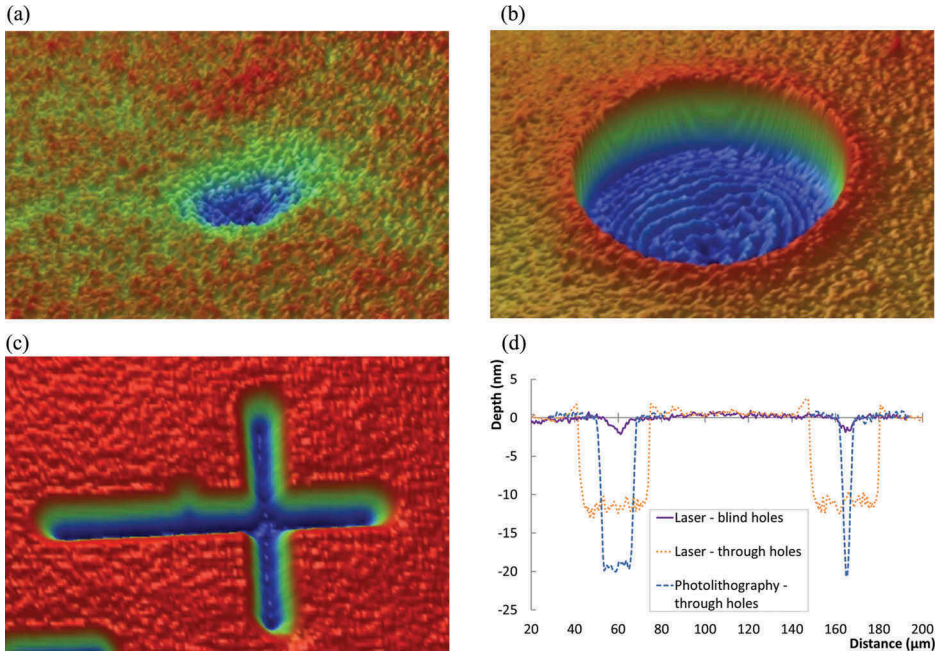

Figure 2. The reconstructed 3D image of the white light interferometry measurement of: (a) a laser patterned blind hole, (b) a laser patterned through hole and (c) a photolithography patterned through feature. (d) The comparison of the cross-section profiles of feature (a), (b) and (c); note the different units on the *x*- and *y*-axis.

time decides the removal depth. In comparison, the laser process essentially melts and vaporises the irradiated ITO region and an incomplete vaporisation is likely to occur due to the insufficient energy coupling. After the laser pulse, the molten ITO forms recast layer on the bottom and edges of the patterned hole. These holes are regarded as through holes as long as the bottom area is not electrically connected.

The bottom of the laser patterned hole was examined by the energy dispersive x-ray (EDX) spectroscopy to confirm the chemical elements of the ITO layer and at the bottom of a through hole. The EDX analysis revealed the presence of the indium and tin elements within the patterned hole, but with a much reduced number of counts compared with the non-patterned ITO region, as shown in Figure 3(a). The evidence suggests that the shallow depth of laser patterned through hole is indeed caused by the ITO recast layer due to the incomplete vaporisation. The SEM image in Figure 3(b) shows distortions in the areas corresponding to the laser patterned through holes as a result of electrons accumulation, which suggests there is no conductivity within these laser patterned through holes.

2.3. SmA material switching and scattering observation

The layered structure of the SmA phase leads to distinct electro-optic properties of the LC materials. Doped ionic species move preferentially between the

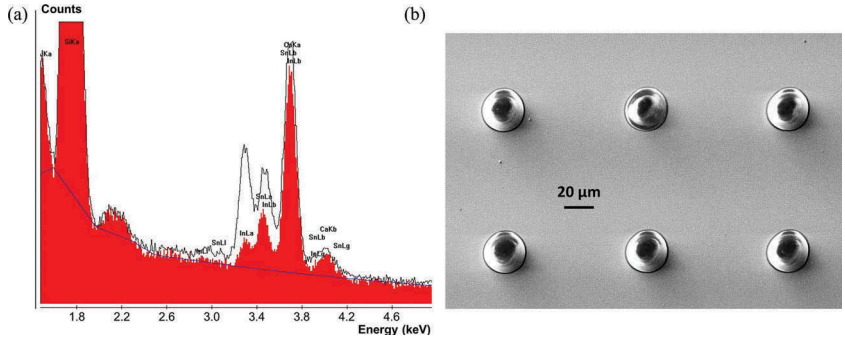

Figure 3. (a) The chemical elements analysis of area inside (red columns) and outside (*black line* profile) of the patterned hole. (b) The SEM image of the laser patterned through holes.

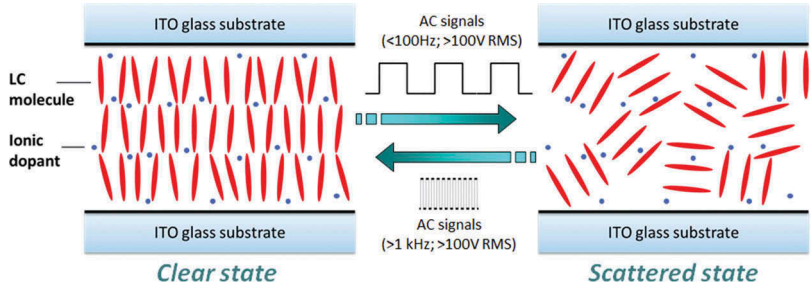

Figure 4. (colour online) Schematics of the cross-section of a SmA LC cell and LC director orientations in the clear (*left*) and scattered (*right*) states.

layers rather than across the layers. In the presence of a low frequency (<100 Hz) and high electric voltage (>100–150 V), the ionic dopant can be forced passing through the SmA layers inducing focal conic defects, which will result in a highly scattered state when the distribution of the LC molecules is sufficiently randomised, as shown in Figure 4. On the other hand, in the presence of a high-frequency electric voltage (>1 kHz) the ionic motion is damped out, resulting in dielectric reorientation of the LC molecules into an aligned state within the layers, causing the LC to appear clear. These two modes of operation create the bi-stable behaviour of the material.

The devices prepared using the patterned and un-patterned electrodes were subjected to AC driving voltage of square-wave pulses and the results were recorded. The test devices were placed between cross-polarisers under a microscope (Olympus BX51, available from Olympus, Tokyo City, Tokyo, Japan) mounted with a high-speed camera (CR600x2, available from Optronis, Kehl, Germany). When test devices are in a clear state, the SmA LC materials are homeotropically aligned along the direction normal to the substrates and the devices appear dark, as light through the device is blocked by the crossed polarisers. When the devices are in the scattered state, the SmA LC molecules are randomised, where the polarisation of the light is changed randomly, such that the devices appear bright under the microscope.

2.4. Transmittance measurement

The in-line transmittance response of the test devices was measured as follows. A red laser (LE07 operating at 650 nm, 1 mW, available from Maplin, Rotherham, UK) was used to illuminate the centre of the test devices. The laser has a 2.8 mm beam aperture such that the average transmittance change was recorded over the same area. The laser beam had a zero incident angle on the testing device. A silicon-based photodiode having a 10 × 10 mm^2 photosensitive area and a response range of 240 – 1100 nm was used to monitor the change in laser intensity through the test device at the direction that is perpendicular to the device plane. The IGOR WaveMetrics (Portland, OR, USA) software was used to generate the driving signals (±10 V maximum) together with a ×20 voltage amplifier (A400D, available from FLC Electronics, Partille, Sweden), such that high voltage driving signals were obtained. The IGOR software was also used to record the analogue signal from the photodiode via a data acquisition card (NI PCI6221 37Pin, Newbury, UK) and convert it into the digital data. The maximum laser transmittance recorded with no device in the beam path was used as a reference, with other measured transmittance normalised with respect to this maximum value. The transmittance decreases as the scattering of the SmA LC devices begins, with the transmittance reaching its minimum value when the device is fully scattered.

3. Results and discussion

3.1. SmA devices with the electrodes patterned by laser ablation

Patterned electrodes prepared by the laser ablation process as described in Section 2.2 were made into devices with the organic SmA LC. The scattering processes of the devices with patterned and un-patterned electrodes were observed and compared. The device transmittance was measured to determine the effective scattering time of the device and the scattering propagation speed, and it was then compared with the calculated values based on the defect growth model. The effect of the surface roughness of the electrodes on the scatter nucleation was investigated.

3.1.1. Scattering propagation

The scattering process for a SmA LC device was observed by an optical microscopy under crossed polarisers. Figure 5 shows the scattering process with

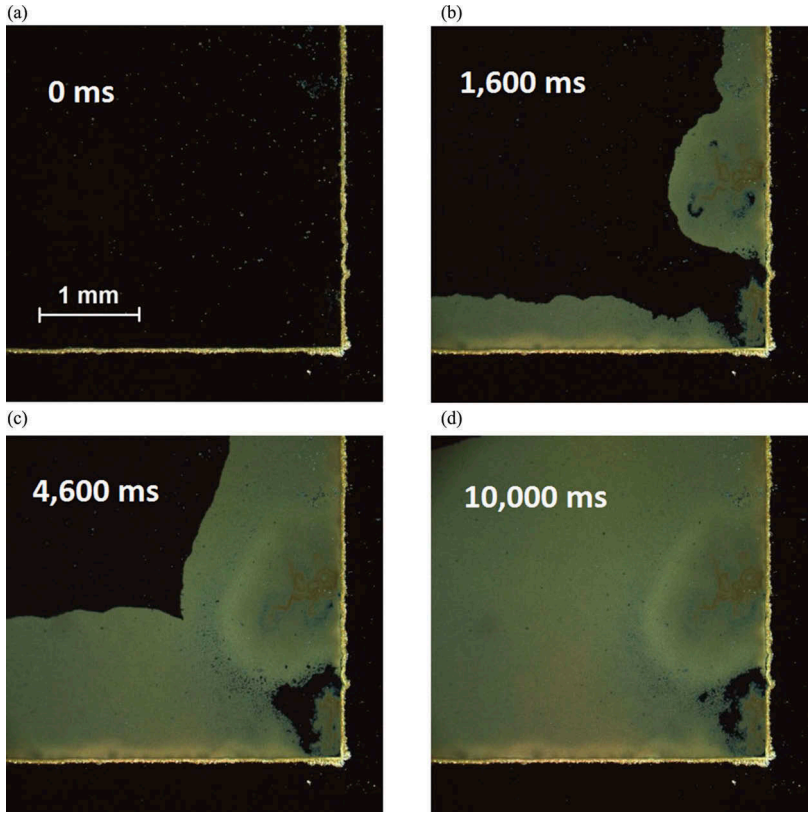

Figure 5. (colour online) (a–d) Images illustrating the scattering process at a corner of a SmA device with un-patterned electrodes in square shape as a function of time with scattered regions grown from the edges of the active electrode when a low scattering voltage of 160 V was applied. The images are of the same scale.

un-patterned electrodes. The images reveal the scattering development and growth of scattered defects with time. The 160 V rms voltage (normally between 180 and 200 V rms are used) square wave at 40 Hz was applied to the device to slow down the scattering process for a better observation. Figure 5(a) shows one corner of the device in the clear state, after the previous rounds of the scattering-clearing. Figure 5(b) and (c) show the initiation and propagation of the scattered regions. It is obvious that the scattering is initiated from the edge of the active region where an electric field gradient was generated under the driving voltages. Figure 5(d) shows a fully scattered state apart from a faulty region which is not fully scattered at the bottom right corner of the device, which is likely to be caused by the ionic dopant depletion in the LC material.

The scattering process for a SmA LC device with through holes patterned by laser ablation in the electrodes was observed and shown in Figure 6. Figure 6(a) shows the device with the through holes in a squared array with a spacing of 100 μm in the clear state. The circular bright areas within the patterned holes are the defects which were resulted from the SmA LCs not being cleared by the previous clearing action. Because of its small scale, such features would not be seen by naked eyes if not using a microscope. Figure 6(b) shows the nucleation of scattered regions. It is apparent that the defects are created initially in the region around the edge of the abrupt through holes which generate a distribution of electric field gradient when voltage signals are applied. The scattering starts uniformly around the edge of a hole and propagates to the rest of the active area, as shown in Figure 6(c–e). Figure 6(d) shows the fully scattered state after the voltages are removed.

In the centre region of a through hole, about 10 μm in diameter, as shown in Figure 6(a), the strength of the electric field is weak and the SmA LC is hardly scattered at the first instance. It may take a while (up to a few tens of seconds sometimes depending on the size of the hole) to appear to be scattered due to the growth/movement of the scattered domains, but it can be fully cleared or scattered, as shown in Figure 6 (a) and 6(f).

It is clear that the LC defect generation or scattering is initiated along the edge of a patterned through holes where both the electrode surface roughness and the lateral electric field gradient are present. We believe

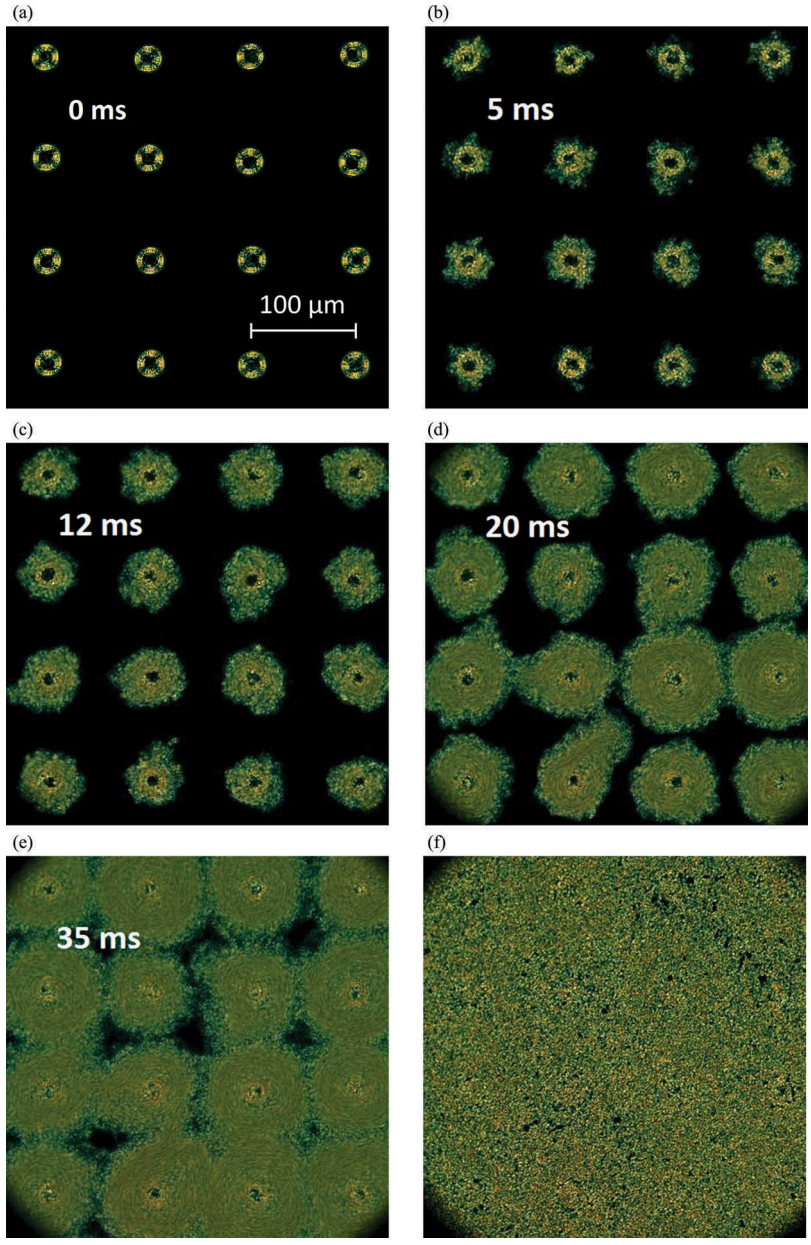

Figure 6. (colour online) (a–f) Images illustrating the defect nucleation and propagation processes of the SmA LC device with the laser patterned through holes with time with a scattering voltage of 200 V rms. The images are of the same scale.

that this is due to the large field gradient, rather than the influence of surface roughness which is important to the scattering threshold voltage.[12]

In order to separate the field gradient effect from the surface roughness effect, samples with blind holes with rough edges similar to that of the through holes were examined. The blind holes are also spaced by 100 µm in both *x*- and *y*-directions, and the corresponding scattering process is shown in Figure 7 with time. The locations of the blind hole are indicated as *dashed circles* in Figure 7(a). The sample with blind holes appears to be completely transparent in the clear state. In Figure 7(b) and 7(c), the scattering propagates from one side and continues until the region under observation is fully scattered, showing no preferential initiation of scattered regions along the edge of the blind holes. A relative low voltage of 160 V rms at 40 Hz was used during the scattering process to allow an easy image capture. The combination of Figures 6 and 7 suggests that the observed scattering is initiated by the field gradient and not the electrode surface roughness.

3.1.2. Device transmittance

The scattering process observed in Figure 6 can be represented by the schematics shown in Figure 8, for

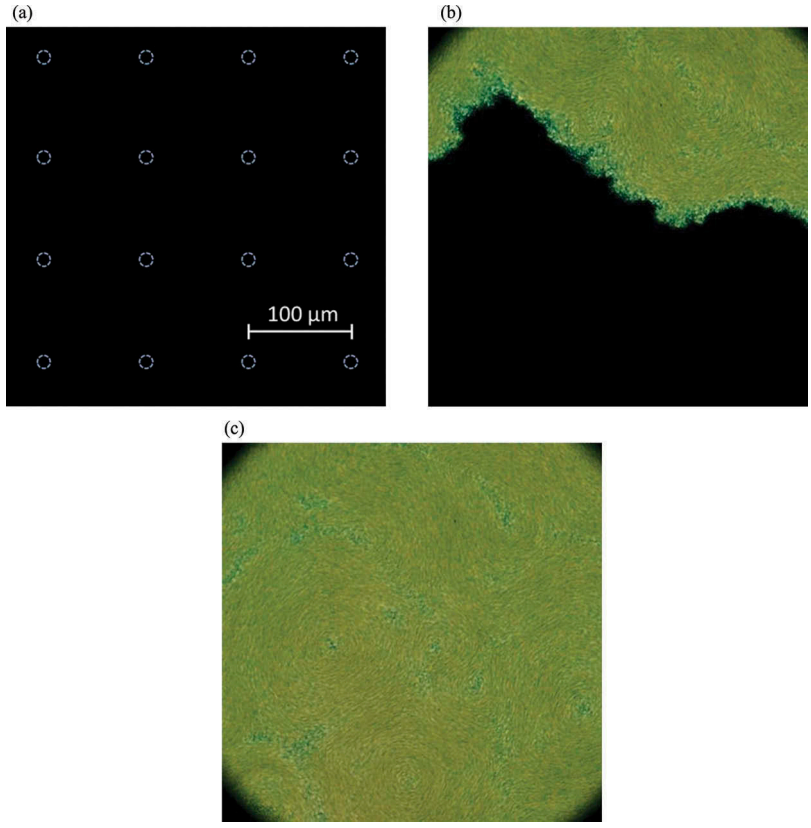

Figure 7. (colour online) Images of (a) a clear state, (b) a half-scattered state and (c) a fully scattered state for SmA LC devices with the electrodes patterned with blind holes. The images are of the same scale.

the calculation of the transmittance with respect to time. Figure 8(a) indicates the moment that the scattering is just about to propagate and it is considered as say time frame 1. Figure 8(b) indicates the moment that the scattering fronts from any patterned holes just merge and it is considered as time frame 2. The moment that the device becomes fully scattered is considered as time frame 3, as shown in Figure 8(c). The laser patterned holes are 30–35 µm in diameter, which is shown as *dotted circles* in Figure 8(a). The scattered defect ring is slightly smaller, with a measured outer diameter of ~27 µm. The electric field close to the edge of a hole is still strong enough to scatter and clear the SmA LC towards the centre of the hole, resulting in a size difference.

The transmittance T of the SmA LC device is calculated as the percentage of the non-scattered area to the overall investigated area that contains the patterned holes. Here, the entire active region is equally divided into multiples squares, the centre square is marked with dashed lines in Figure 8. Each square is of 100 × 100 µm^2 and it contains one through hole in the centre. The scattering process for the entire active region is the same in each square, so only one such square is considered for the ease of calculation. The scattering propagation speed is assumed to be constant and equal in all propagation directions. At time frame 1, the transmittance is

$$T_1 = T_0 - T_0\left(\frac{A_{\text{defect}}}{A_{\text{overall}}}\right) \times 100\% \tag{1}$$

where T_0 is the initial transmittance of SmA LC device in the clear state which takes into account the transmittance loss (~17–19%) due to device reflectivity and absorptivity. Any subsequent change in the transmittance due to the SmA LC scattering will be based on the T_0 value. A_{overall} is the area of the investigated square, A_{defect} is the area of the scattered defect ring, and it is calculated with the following equation:

$$A_{\text{defect}} = \pi \times \left(r_{\text{defect}}^2 - r_{\text{dead}}^2\right) \tag{2}$$

r_{defect} is the outer radius of the defect ring, r_{dead} is the radius of the 'dead' region and is also the inner radius of the defect ring. When the scattering front propagates, the transmittance between time frames 1 and 2 is calculated as:

$$\begin{aligned} T_{1-2} &= T_1 - T_0\left(\frac{\Delta A_{\text{scatter}}}{A_{\text{overall}}}\right) \times 100\% \\ &= T_1 - T_0 \times \pi \times \frac{\left(r_{\text{scatter}}^2 - r_{\text{defect}}^2\right)}{A_{\text{overall}}} \times 100\% \end{aligned} \tag{3}$$

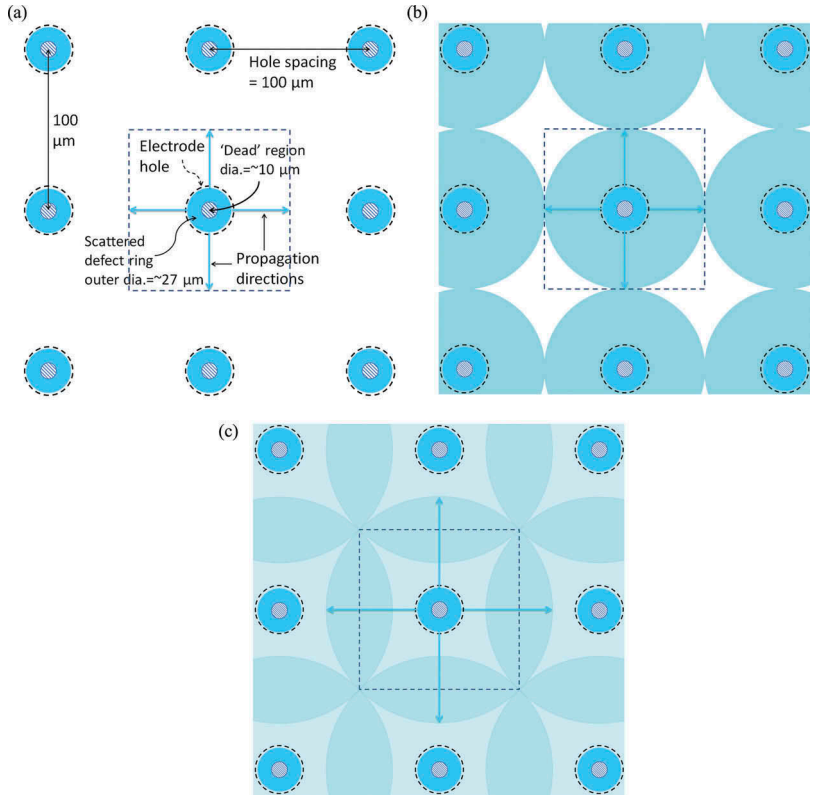

Figure 8. (colour online) Schematics of the SmA device active region with 100 μm spaced holes: (a) at time frame 1, the beginning of scattering cycle; (b) at time frame 2, when the circular scattering front starts to merge; and (c) at time frame 3, when the device becomes fully scattered.

where $\Delta A_{\text{scatter}}$ is the area change due to the scattering growth. After the scattering front just merges, that is $r_{\text{scatter}} \geq 50$ μm, the transmittance between time frames 2 and 3 becomes

$$T_{2-3} = T_1 - T_0 \times \frac{\left(\Delta A_{\text{scatter}} - A_{\text{overlap}}\right)}{A_{\text{overall}}} \times 100\% \qquad (4)$$

where A_{overlap} is the area of scattering overlap within the 100 × 100 μm^2 square from all four neighbouring scattering centres.

The transmittance of the SmA LC device with the patterned through holes (100 μm spaced) was recorded as shown in Figure 9, with the experimental setup as described in Section 2.4. The scattering driving signal is delivered to the device at 0.1 s and the transmittance decreased to a few percent after ~0.075 s (scattering time). The values are read from the recorded transmittance curve (red line) instead of the fitted curve (blue line) as shown in Figure 9(b). The scattering time includes the defects nucleation

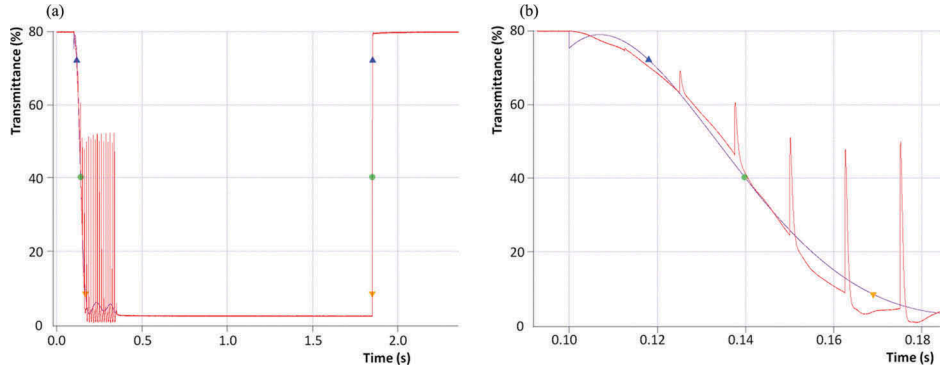

Figure 9. (colour online) (a) The recorded transmittance of a SmA LC device with the patterned through holes (100 μm spaced) during one scattering-clearing cycle. (b) The zoomed-in region of the transmittance curve in Figure 8(a) during the scattering process.

and scattering propagation process as shown in Figure 6. The scattering signal was at 180 V rms and 40 Hz and there were 10 pulses. The appearance of spikes in the transmittance curve during the scattering was a result of change in the voltage polarisation. The transmittance was maintained at the same level after the voltage was removed. When the clearing voltage (10 pulses at 150 V and 2 kHz) was applied, the transmittance increased rapidly to its initial value of 80% as shown in Figure 9(a).

The transmittance data during the scattering process in Figure 9(b) are replotted as the scattering variation ($1 - T - T_{min}$) against the time squared, as shown in Figure 10. T_{min}, a few percent, is the minimum transmittance when the device is in the fully scattered state. As a result, the fully scattered state is considered as $1 - T_{min}$ and the fully cleared state is considered as 0%. The transmittance spikes due to the voltage polarisation change are ignored. The curve starts at ~20% because of the light loss through the physical SmA LC device. The calculated transmittance T, based on Equations (1–4) and a constant speed of 0.68 mm/s, is also plotted on the same graph over the time frames 1–3. The speed is calculated from the measured data as the average speed of the scattering front. The measured and calculated curve matches each other very closely and it proves that the scatter propagation speed is indeed constant and the same in all scattering propagation directions.

Between 0 and 1500 ms^2 in Figure 10, the calculated curve increases slightly faster than the measured curve probably because the scatter nucleation process was not considered in the calculated data. Such a nucleation process can be neglected according to Figure 9(b), only a few milliseconds compared with the scatter propagation time.

3.1.3. Scattering time

The scattering time Δt was recorded from a cleared state to a scattered state when the measured transmittance changes from 90% to 10% of the value T_0. The SmA LC devices are switched between the scattered and clear states repetitively when the measurements are taken. For scattering, 10 pulses of signal at 40 Hz from 160 to 200 V rms were used; for clearing, 10 pulses of signal at 2 kHz and 150 V rms were used. Four SmA LC devices are compared, one un-patterned and three patterned with through holes of different spacings, 100, 250 and 500 μm, respectively. The largest propagation distance (Δd_{max}, indicated in an inset in Figure 11) of the scattering front is calculated as the distance travelled from the edge of the defect ring until the device is fully scattered and it depends on the hole spacing. They are ~55 μm for the 100 μm spaced holes, ~162 μm for the 250 μm spaced holes, ~339 μm for the 500 μm spaced holes and ~1400 μm for the un-patterned device due to the size of the laser beam used in the transmittance measurement.

The variations in the scattering time of organic SmA LC devices with various Δd_{max} are shown in Figure 11. For all cases the scattering time decreases as the applied voltage increases. It is also noticeable that under the same driving conditions, the scattering time is shorter for a shorter propagation distance. As an example, the scattering time of the un-patterned device (~1400 μm propagation distance) is roughly more than twice as long as the device with the ~55 μm propagation distance under the investigated scattering voltages. The difference in the scattering time is not in proportion with the difference in the propagation distance, this is evaluated in terms of propagation speed in Section 3.1.4.

Scattering times with the applied voltage (180 V rms at 40 Hz) were also measured to determine the effect of blind holes compared with through holes. For the

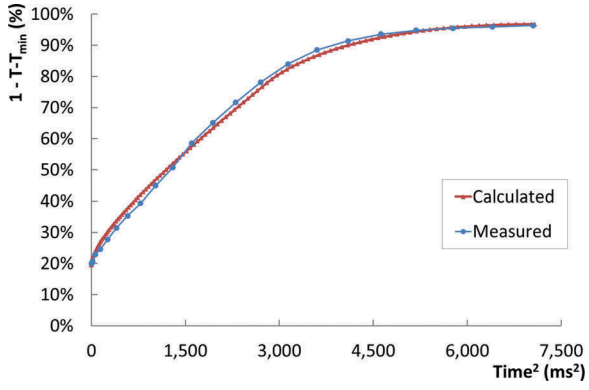

Figure 10. (colour online) The measured and calculated transmittance data plotted as ($1 - T - T_{min}$) with respect to the time squared.

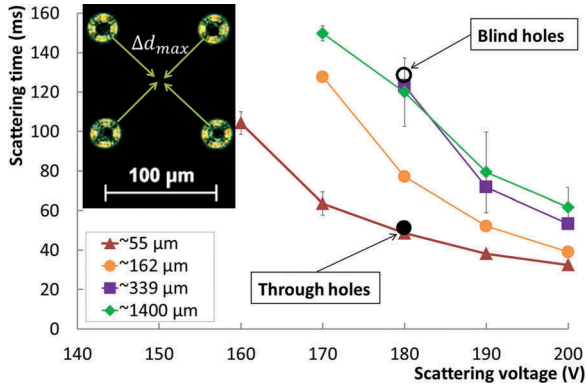

Figure 11. (colour online) Variation in scattering time of organic SmA LC devices for various Δd_{max}.

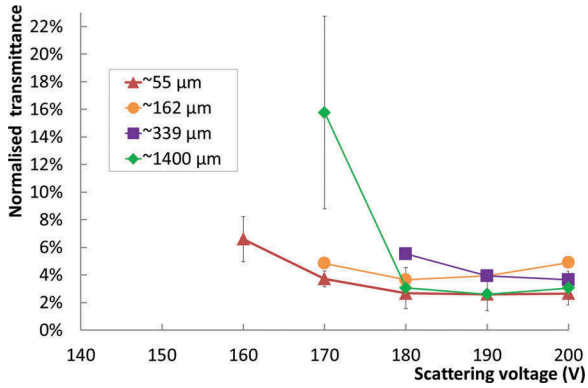

Figure 12. (colour online) Variation in optical transmittance in the scattered state of organic SmA LC devices for various Δd_{max}.

sample with through holes, the switching time was ~50 ms, whereas for the sample with blind holes it was ~130 ms, which is consistent with the relationship between the patterned and un-patterned devices, as shown in Figure 12. The comparable scattering time between the un-patterned device and the device with blind holes confirms that the field gradient is responsible for the creation of randomised domains in the SmA LC material not the surface roughness.

The optical transmittance was measured for the devices with various Δd_{max} after they were fully scattered, as shown in Figure 12. The transmittance is more consistent in the devices comprising the patterned electrodes. In particular at low driving voltages (160/170 V) the patterned devices achieved much lower and more uniform transmittance values (< 8%) than the un-patterned devices. The un-patterned device cannot be visibly scattered evenly at 160 V rms due to the inconsistent scattering.

The results therefore show that the reduced scattering time and more consistent transmittance values can be achieved for the SmA LC devices comprising patterned electrodes. These results were based on the comparison of small glass cells with an active region of 10 × 10 mm^2. It is therefore to be expected that the scattering process will be even slower for larger un-patterned LC devices as the propagation time will increase with the longer distance from the edge of the device to the centre. In comparison, the scattering of the patterned devices started from the disruptive patterns in the electrodes, and the propagation time will therefore be dependent on the pattern density/spacing. In addition, the patterned devices can be scattered with the lower scattering voltage, hence the unlikely occurrence of a breakdown or arcing from the impurities in the LC.

3.1.4. Scatter propagation speed

The scatter propagation speed s is defined as the speed of the scattering front movement normal to its front line. It can be calculated as a ratio of the distance Δd, that the scattering front travelled when transmittance decreases from 90% to 10% of T_0, to the measured scattering time Δt. Based on Equation (3), the Δd is calculated as 34.5 µm for the Δd_{max} of 55 µm, 93 µm for the Δd_{max} of 162 µm, 189 µm for the Δd_{max} of 339 µm and 885 µm for the un-patterned devices. The speed s for the un-patterned devices is much larger than the patterned devices. This resulted from the fact that there are impurities observed in the organic-based SmA LC which causes scattering nucleating not just from the edge but also from the impurities themselves, as shown in Figure 13. Hence the s value for the un-patterned devices was not correct and is not used in the calculation.

The calculated average s values for the patterned devices are plotted with respect to the scattering voltage in Figure 14 and there is a linear increase

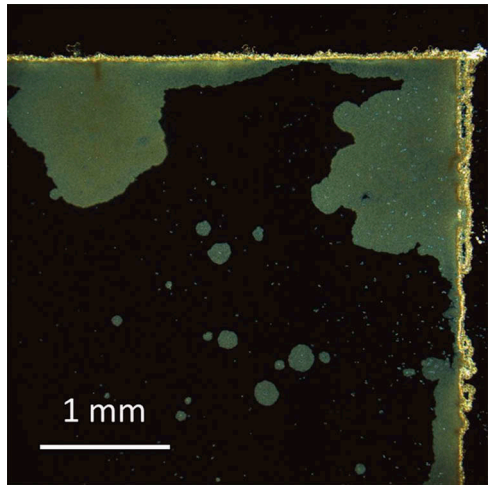

Figure 13. (colour online) An image with the scattering originated from both the edge of the active region as well as the impurities in an organic SmA LC device.

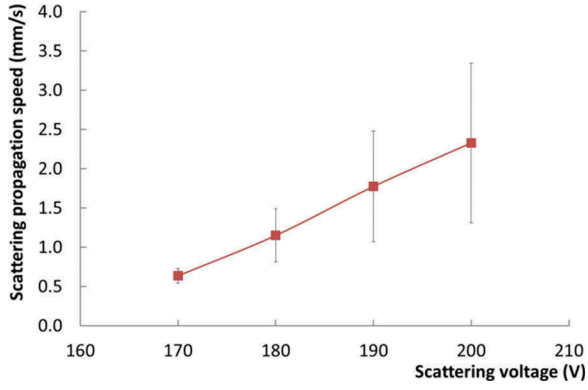

Figure 14. (colour online) Calculated scattering propagation speed of organic SmA LC devices at varying scattering voltages.

relationship between the two parameters. The large error bars are from the large calculated *s* values for the devices with longer scattering propagation distance. It is thought that the scattering from the impurities is likely to occur when there is a large space between the patterned through holes, hence reducing the average propagation time.

Assuming there is no scattering from the impurities of organic SmA LC materials, that if one is to assemble a device of 1 × 1 m^2 for the large window sized panel. It will take 250 s to fully scatter the unpatterned device, meanwhile it will only take ~177 ms to scatter the patterned device with 500 µm spaced through holes or ~35 ms with 100 µm spaced holes, yielding an improvement of several thousand times in the scattering time. However, the spacing between two neighbouring features cannot be too small, or the scattered defect rings start to deteriorate the transmittance of the device in the clear state. The transmittance will drop more than 10% if the spacing is less than 70 µm under the same investigated condition.

3.2. SmA devices with the electrodes patterned by photolithography

Patterned electrodes with different shaped features prepared by the photolithography process described in Section 2.2 were made into devices with the siloxane-based SmA LC. The scattering process and scattering time were observed and measured, whereas the results on the effects of photolithography patterned features are presented and discussed in the following sections.

3.2.1. Scattering propagation

Figure 15(a) shows the siloxane-based SmA LC device in the clear state with the different patterned features (*circled areas*) in the electrode layer. The scattering process was observed and the results are shown in Figure 15(b–d) with increasing number of driving pulses at 150 V rms and 40 Hz. Similar to the device with laser patterned through holes, the scattering is initiated from the edge of the photolithography patterned features and propagates to the rest of the active region. It is clear that neither the method used to pattern the electrode nor the pattern shape have a

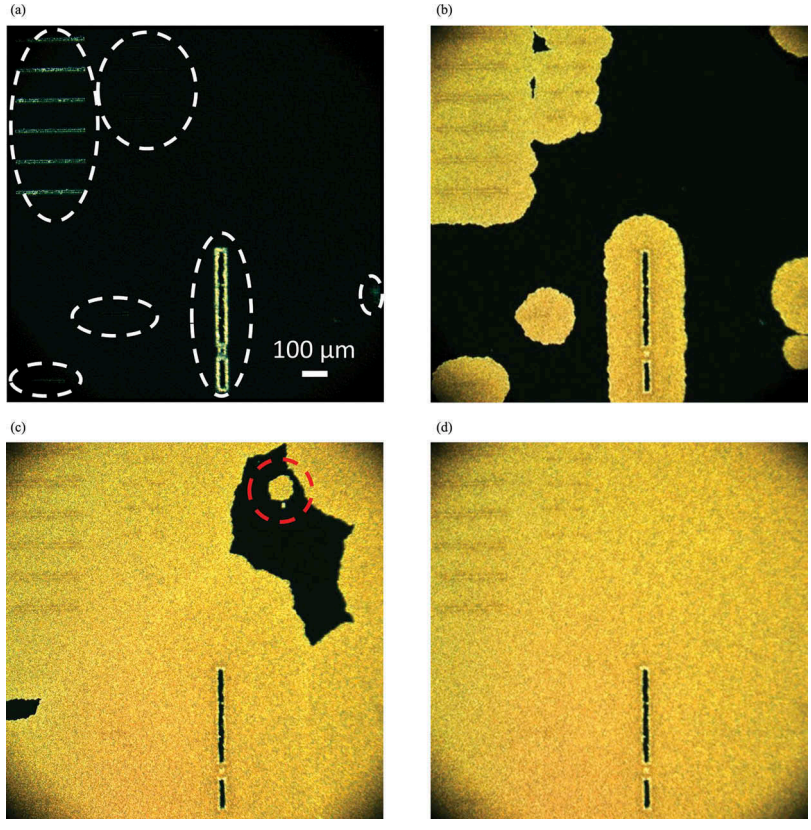

Figure 15. (colour online) (a–d) Scattering process (uniformly nucleated from the defect generation sites along the edges of the photolithography patterned features) with increasing number of driving pulses for the siloxane-based SmA LC device.

detrimental impact on the scattering behaviour of these SmA LC devices.

In Figure 15(c), there is a scattering point circled in red that was not nucleated from the patterned feature, but from the material itself. The siloxane-based SmA LC provided by Dow Corning is engineered to have a less-perfect layered structure, so that scattering can be nucleated from the material itself. The device has more of such scatter nucleation points, but they appeared at a later time than the scattering nucleated by the field gradient effect as can be seen from Figure 15.

3.2.2. Scattering time measurement

Scattering times were measured for the un-patterned and patterned devices when they were switched between the scattered and clear states. For scattering, 10 pulses at 40 Hz at voltages from 150 to 180 V rms were used. For clearing, 10 pulses at 2 kHz and 150 V rms were used. The largest propagation distance Δd_{max}, indicated in an inset in Figure 16, is measured for the area of investigation. They are ~180 µm for the patterned device and ~1400 µm for the un-patterned device.

As seen from Figure 16 that for both devices the scattering time decreases as the applied voltage increases. The scattering time is similar for the un-patterned and patterned devices except for the ones measured at 160 V rms. The similarity confirms that for the siloxane-based SmA LC, the scatter nucleates from the material itself all over the active region. However, the patterned devices show a much lower transmittance in the scattered state at the lower voltages than the un-patterned devices, as shown in Figure 17. The low transmittance was also accompanied by a more consistent scattering performance, shown as the small error bar for the patterned device at 150 V rms. This suggests that the scattering is

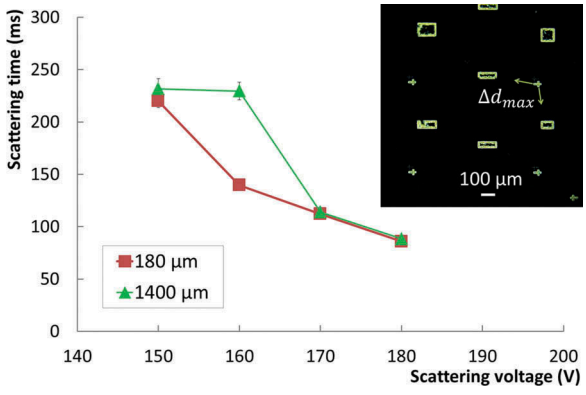

Figure 16. (colour online) Variation in the scattering time for the un-patterned and patterned (photolithography) siloxane-based SmA LC devices.

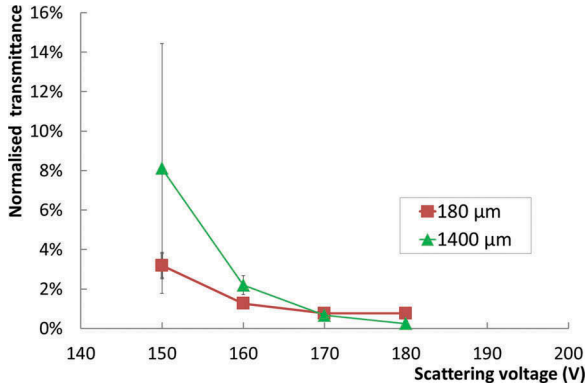

Figure 17. (colour online) Variation in optical transmittance in the scattered state for the un-patterned and patterned (photolithography) siloxane-based SmA LC devices.

nucleated with much ease at low voltage because of the field gradient effect.

The above results show that the photolithography patterned electrodes with different shaped features and smooth and well-defined cross-sections can also initiate scattering from the feature edges as the laser patterned through holes. This confirms that the shape and the cross-section profile of the patterned feature do not affect the scattering initiation as long as there is the discontinuity in the conductive layer, ITO in this case, which will generate a strong enough electric field gradient.

4. Conclusions

In this study, we have developed a method that enables organic SmA LC devices to switch uniformly and hence fast from a clear state to scattered state. The reduced scattering time for the organic SmA LC devices is demonstrated by having uniformly patterned features in the ITO layer of the glass substrate. As a result, the scattering nucleates from the defect generation sites and propagates until the device is fully scattered. For a 1 × 1 m^2 device, it will take several tens of milliseconds to fully scatter the patterned device, compared with several hundreds of seconds for the un-patterned device. The study proved the concept that it is the electric field gradient effect, rather than surface roughness effect, which initiates the scattering, so the patterned features need to create discontinuities of any shapes in the conductive layer instead of the surface roughness. The patterned devices can also achieve a good and consistent scattered state at lower scattering voltages, hence reducing the operating voltages and the chances of LC arcing under large electric signals.

For siloxane-based SmA devices, it is observed that the scattering can also be nucleated from the patterned

features and resulted in a more uniform scattering. The scattering time for both the patterned and un-patterned devices is similar because the siloxane-based SmA LC used has additives to assist the defect generation for scattering. Nevertheless, the patterned devices show a more uniform scattering and evidence demonstrates that especially at low scattering voltages, it is much easier to initiate scattering from the patterned features. The fully scattered state is also much more repeatable for the patterned device at low voltages.

Fast and uniform scattering of the SmA LC devices with the consistent performance in the scattered state even at lower driving voltages will help to accelerate the adoption of large-size SmA LC panels for light radiation control and projection displays. Other applications such as privacy partition or ambient control for healthcare and office environment can also benefit from using smart windows instead of curtains or fabric screens in a more intelligent and hygienic way.

There are areas which can be further investigated. The diameter of the patterned features is limited to ~30 μm for laser-processed through holes; smaller features could be tested to identify the threshold pattern dimension for the generation of the field gradient effect in the 10 μm thick LC layer devices. The blind holes created are only several nanometres deep, partly due to the laser system controllability and the thin ITO layer which is needed for the better transmittance. It will be interesting to produce deeper blind holes with a different laser system or other techniques, such as the focused ion beam, for a better depth control. Nonetheless, the laser patterning process of through holes as used in this study is fast, easy to control and suitable for a roll-to-roll fabrication of the large plastic SmA LC panels.

Acknowledgements

The authors thank Dr Anthony Davey for providing the organic SmA LC and Dow Corning Corp. for providing the siloxane-based SmA LC used in this study. The authors also thank Dr Stuart Speakman for the helpful discussions.

Disclosure statement

No potential conflict of interest was reported by the authors.

Funding

The UK Engineering and Physical Sciences Research Council (EPSRC) provided the support through the Platform Grant for Liquid Crystal Photonics [grant number EP/F00897X/1].

ORCID

Daping Chu http://orcid.org/0000-0001-9989-6238

References

[1] Wang J. New applications of 3G switchable film face huge markets. Paper presented at: International Convention and Tradeshow of Energy Harvesting Europe; 2014 April 1–2; Berlin, Germany.
[2] Baetens R, Jelle BP, Gustavsen A. Properties, requirements and possibilities of smart windows for dynamic daylight and solar energy control in buildings: a state-of-the-art review. Sol Energy Mater Sol Cells. 2010;94:87–105. DOI:10.1016/j.solmat.2009.08.021.
[3] Park S, Hong JW. Polymer dispersed liquid crystal film for variable-transparency glazing. Thin Solid Films. 2009;517:3183–3186. DOI:10.1016/j.tsf.2008.11.115.
[4] Cupelli D, Pasquale NF, Manfredi S, et al. Self-adjusting smart windows based on polymer-dispersed liquid crystals. Sol Energy Mater Sol Cells. 2009;93:2008–2012. DOI:10.1016/j.solmat.2009.08.002.
[5] Coates D. Polymer-dispersed liquid crystals. J Mater Chem. 1995;5:2063. DOI:10.1039/jm9950502063.
[6] Li L, Tang B, Wang SG, et al. Multifunctional window glazing. SPIE Newsroom; Illumination & Displays [Internet]. 2008 [cited 2016 Jan 9]. Available from: http://spie.org/newsroom/technical-articles-archive/11-1200/1102-multifunctional-window-glazing
[7] Wang CH, Wu CC, Yang YT, et al. Reverse-mode polymer-stabilized dual-frequency cholesteric texture cell for dual mode operations. J Disp Technol. 2012;8(11):663–668. DOI:10.1109/JDT.2012.2215838.
[8] Ma J, Shi L, Yang D-K. Bistable polymer stabilized cholesteric texture light shutter. Appl Phys Express. 2010;3:021702. DOI:10.1143/APEX.3.021702.
[9] Kumar P, Kang S-W, Lee SH. Advanced bistable cholesteric light shutter with dual frequency nematic liquid crystal. Opt Mater Express. 2012;2(8):1121–1134. DOI:10.1364/OME.2.001121.
[10] Lee KM, Tondiglia VP, White TJ. Bistable switching of polymer stabilized cholesteric liquid crystals between transparent and scattering modes. MRS Commun. 2015;5:223–227. DOI:10.1557/mrc.2015.40.
[11] Li L, Li JF, Faris SM, assignee. Electro-optical glazing structures having scattering and transparent modes of operation and methods and apparatus for making the same. United States patent US 7009665 B2. 2003 Dec 24.
[12] Coates D, Crossland W. Electrically induced scattering textures in smectic A phases and their electrical reversal. J Phys D Appl Phys. 1978;11:2025–2034. DOI:10.1088/0022-3727/11/14/012.
[13] Crossland WA, Davey AB, Chu DP, et al. Handbook of liquid crystal: vol 8, applications of LCs, part 1, display devices. Weinheim: Wiley-VCH; 2014. p. 1–33.

[14] Gardiner DJ, Morris SM, Coles HJ. High-efficiency multistable switchable glazing using smectic A liquid crystals. Sol Energy Mater Sol Cells. 2009;93:301–306. DOI:10.1016/j.solmat.2008.10.023.

[15] Hannington JP, Clapp TV, Nishida F, et al., Inventor; Dow Corning Corporation, Cambridge Enterprise Ltd., assignee. Oligosiloxane- modified liquid crystal formulations and devices using same. United States patent US 8368831 B2. 2007 Oct 19.

[16] Newton J, Coles H, Hodgeb P, et al. Synthesis and properties of low-molar-mass liquid-crystalline siloxane derivatives. J Mater Chem. 1994;4:869–874. DOI:10.1039/jm9940400869.

[17] Leadbetter A, Frost J, Gaughan J, et al. The structure of smectic A phases of compounds with cyano end groups. J Phys. 1979;40:375–380. DOI:10.1051/jphys:01979004004037500.

[18] Li L, Jones CD, Magolan J, et al. Siloxane-terminated phenylpyrimidine liquid crystal hosts. J Mater Chem. 2007;17:2313. DOI:10.1039/b700972k.

[19] Xu H, Davey AB, Crossland WA, et al. UV durable colour pigment doped SmA liquid crystal composites for outdoor trans-reflective bi-stable displays. In: Khoo IC, editor. Proceedings of SPIE 8475; 2012 Oct 11; San Diego (CA). Liq Crys. XVI(847506):1–8. DOI:10.1117/12.928025

[20] Gardiner DJ, Coles HJ. Organosiloxane liquid crystals for fast-switching bistable scattering devices. J Phys D Appl Phys. 2006;39:4948–4955. DOI:10.1088/0022-3727/39/23/008.

[21] Clapp TV, Crossland WA, Davey AB, et al., Dow Corning Corporation, Cambridge Enterprise Limited, assignee. Liquid crystal formulations and structures for smectic A optical devices. United States patent US 8956548 B2. 2011 Mar 15.